Version of Record: https://www.sciencedirect.com/science/article/pii/S0009250923011892
Manuscript_143a326fd2da3f5121422879b9c48da6

# Experimental study of transient particle suspension in bioreactors using a light attenuation technique

Charlotte Maillot[a], Angélique Delafosse[c], Natalia De Isla[b], Eric Olmos[a], Dominique Toye[c]

[a] *Université de Lorraine, CNRS, LRGP, F-54000 Nancy, France*
[b] *Ingénierie Moléculaire et Physiopathologie Articulaire, Université de Lorraine, CNRS UMR 7365, 54500 Vandoeuvre-lès-Nancy, France*
[c] *Department of Chemical Engineering – Product Environment and Processes (PEPs), Université de Liège, Belgium*
[d] *Corresponding author: Eric Olmos (eric.olmos@univ-lorraine.fr)*

## Abstract

The culture of mesenchymal stromal cells relies on the use of suspended microcarriers as adhesion supports. During the particle suspension phases, the temporal evolution of the spatial distribution of particle concentrations is generally poorly characterized. In this study, the light attenuation technique was used to access this distribution and the duration of particle homogenization. Considering the minimal agitation rate $N_{ref}$ for which particle suspension was observed for all the microcarrier concentrations $\langle C \rangle$ studied, the results showed that using an agitation frequency close to $N_{ref}$ significantly increased the homogenization duration compared to $N \simeq 1.7 \times N_{ref}$. The transient microcarrier overconcentration was also determined locally. At $N = N_{ref}$, the resuspension time was negatively impacted by $\langle C \rangle$, which also resulted in longer particle overconcentrations. A time-integral particle overconcentration term was considered to estimate the severity of inter-microcarrier collisions. The results suggested that increased agitation could limit time-cumulative overconcentrations beyond a particle concentration of 3 g/L.

*Keywords:* Light attenuation technique ; bioreactor ; microcarrier ; suspension

## 1. Introduction

In recent years, Mesenchymal Stromal/Stem Cells (MSCs) have been increasingly used in regenerative medicine and Advanced Therapy Medicinal Products (ATMPs). These products have been shown to address various indications such as immune/auto-immune diseases, bone and cartilage regeneration, heart or neuro-degenerative diseases (Maillot et al., 2021) but the success of these therapies still depends on the design of efficient bioproduction process. In the food industry, stem or primary cells are also a very interesting cell source for the production of cultured meat. In order to increase production capacities of MSCs and

reduce their costs, the culture of MSCs in stirred tank reactors (STR) is progressively gaining ground alongside 2D planar static cultures in T-Flasks which allow little online culture parameter controls despite the increased complexity of the physical mechanisms encountered (hydromechanical stress, gas dissolution, mixing) (Simaria et al., 2014; Wyrobnik et al., 2020; Nienow et al., 2016a; Jossen et al., 2016). In STR, MSCs are generally adhered to microcarriers that are suspended following stirring procedures that are mainly empirically established. First, since anchorage-dependent mechanisms are expected to last between 5 and 20 minutes from a biological point of view (Wysotzki et al., 2020), MSC expansion on microcarriers requires an initial adhesion phase during which the MSCs and microcarriers settle to the bottom of the tank. In contrast, once the cells have successfully adhered to the carriers, homogenization is preferred from a process perspective to limit aggregation and reduce metabolic gradients, including nutrient concentrations, metabolic by-products, but also to ensure sufficient aeration and pH control. The nature of the process therefore results in an inevitable phase where microcarriers settle to the bottom of the tank and are subsequently suspended. In addition, once the microcarriers are fully colonized (typically after several days of expansion), it is possible to continue the expansion process by adding fresh microcarriers and using bead-to-bead cell transfer (Sion et al., 2021). For the same reasons, cell transfer from colonized microcarriers to fresh carriers requires sedimentation of the solid phase and resuspension after successful cell migration. Typically, a minimal agitation rate to suspend all the particles $N_{js}$ is set in the bioreactor during microcarrier-based expansion processes in order to (1) limit shear stress which may compromise cell viability and functionality (Papoutsakis, 1991; Stolberg and McCloskey, 2009; Yourek et al., 2010), yet also (2) guarantee particles are in suspension and limit aggregation (Ferrari et al., 2012; Yuan et al., 2014) while ensuring sufficient homogenization and efficient mass transfer although this choice remains although largely empirical. Physical interactions between the particles are expected to have significant effects on the cells expanded on these growth supports; for example, it has been shown that mechanical stresses, including shear and collision forces, affect the growth and phenotypic attributes of cells such as human mesenchymal stem cells (Harburger and Calderwood, 2009; Discher et al., 2005; Yourek et al., 2010; Maillot et al., 2022). More recently, it was also established that the production of extracellular vesicles by cells is related to the hydromechanical stresses (Piffoux et al., 2019; Grangier et al., 2020). For all these reasons, it is important to understand the particle interactions mechanisms during the phases of resuspension in order to determine the stresses to which the cells may

be submitted (which may occur several times during culture).

To date, few studies have characterized microcarrier mixing in STRs applied to microcarrier-based cell cultures. Mixing times in the Mobius CellReady bioreactor equipped with a marine impeller were determined for working volumes of 1 and 2.4 L with Solohill collagen-coated microcarriers (Sartorius, Germany) at concentrations of 15 and 30 g $L^{-1}$ (Grein et al., 2016). In addition, mixing time in a vertical wheel system was determined for in comparison with STR (Sousa et al., 2015). Although these studies provide information on how mixing time is affected by parameters such as agitation, particle concentration and bioreactor size, the evaluation of mixing mechanisms and in particular concerning aspects of physical stress that cells may perceive remains limited due to the difficulty of assessing the distribution of particle concentrations. For instance, to our knowledge, the evaluation of a 'local over-concentration factor' applied to the microcarrier suspension in STRs used for MSC cell culture would be new and informative for this specific process.

This work presents the possibility of using light attenuation measures to detect local particle concentrations during the transient suspension of microcarriers in a STR. Briefly, a LED backlight can be used to illuminate a tank which is placed in a cubic aquarium filled with water to minimize optical deformation. Compared to other techniques, the light attenuation technique offers the combined advantages of (i) being a non-intrusive technique, (ii) measuring instantaneous 2D maps of particle concentrations, (iii) being easy to implement. However, it relies on the use of transparent or translucent particles. A more detailed discussion of the advantages and disadvantages of this technique as well as other techniques that are commonly developed in the literature can be found in Delafosse et al. (2018). Although this previous work was using this technique to characterize of the spatial distribution of particle concentrations once the steady-state was reached, the transient state between particle settling and steady state has not yet been characterized. More precisely, this technique is used here to characterize particle suspension kinetics, resuspension times and concentration distributions during resuspension phase. The results obtained were also combined with a previously published collision model to assess the possibility of cell damage during the resuspension step. Thus, these results not only provide new data on the transient particle suspension but should also be useful for the development of MSC culture processes, in particular for the adaptation of the agitation conditions applied to MSC cultures.

## 2. Material and method

### *2.1. Experimental setup*

All experiments were performed in a tank which is a cylindrical container with a diameter of $T$ of 12 cm and a hemispherical bottom (Pierre Guerin Tryton). The maximum working volume of the tank is of 1.12 L but the working volume used in this study was of 700 mL as this volume has previously been used to successfully expand mesenchymal stem cells on microcarriers (Sion et al., 2021). Liquid homogenization and particle suspension was ensured by a down-pumping HTPG impeller with a diameter $D$ of 6 cm and an off-bottom clearance $Cl$ of 6 cm. Accordingly the ratios $D/T$ and $Cl/T$ were equal to 0.5 and 1 respectively. When used for cell culture, the bioreactor is equipped with four online probes that allow the monitoring of temperature, pH, dissolved oxygen and viable cells. 3-D printed elements of the same size and shape as these probes were thus placed in identical locations in such as way as to obtain similar liquid and particle flows (see Figure 1) . The solid phase consisted of Cytodex 1 microcarriers (Cytiva Life Sciences) which are made of cross-linked dextran matrix which is substituted with positively charged N-diethylaminoethyl groups. These microcarriers swell when placed in a saline solution ; in a phosphate buffer saline (PBS) solution at a concentration of 0.01 M, their density and mean hydrated diameter were 1030 kg $m^{-3}$ and 180 µm respectively .

### *2.2. Light attenuation technique*

After verification of back-light stability between experiments, calibration was performed with Cytodex 1 microcarrier concentrations ranging from 0 to 37.5 g $L^{-1}$ according to the methods previously described (Delafosse et al., 2018). More precisely, the resuspension experiments of Cytodex-1 microcarriers were carried out for concentrations of 2.5, 3.75, 5, 7.5, 10, 12.5 and 15 g/L, which corresponded to available surface areas available of 12, 18, 24, 36, 48, 60, 72 $cm^2$/mL. The reference agitation rate was $N_{ref} = 70$ rpm was defined as the minimal agitation rate ensuring the complete suspension of the microcarriers, whatever the concentration considered. Agitation was set at 120 rpm ($1.7 \times N_{ref}$) to achieve a rapid homogeneous suspension of the particles during calibration. For each microcarrier concentration studied, a 30-second video was used for the calibration with an acquisition frequency of 2.5 Hz and an acquisition window of 761×1100 pixels, corresponding to a spatial resolution of approximately 0.12 mm (see Figure 1). Gray levels of each pixel in the images recorded by the camera were related to the local volume fraction of the particles. It was assumed that

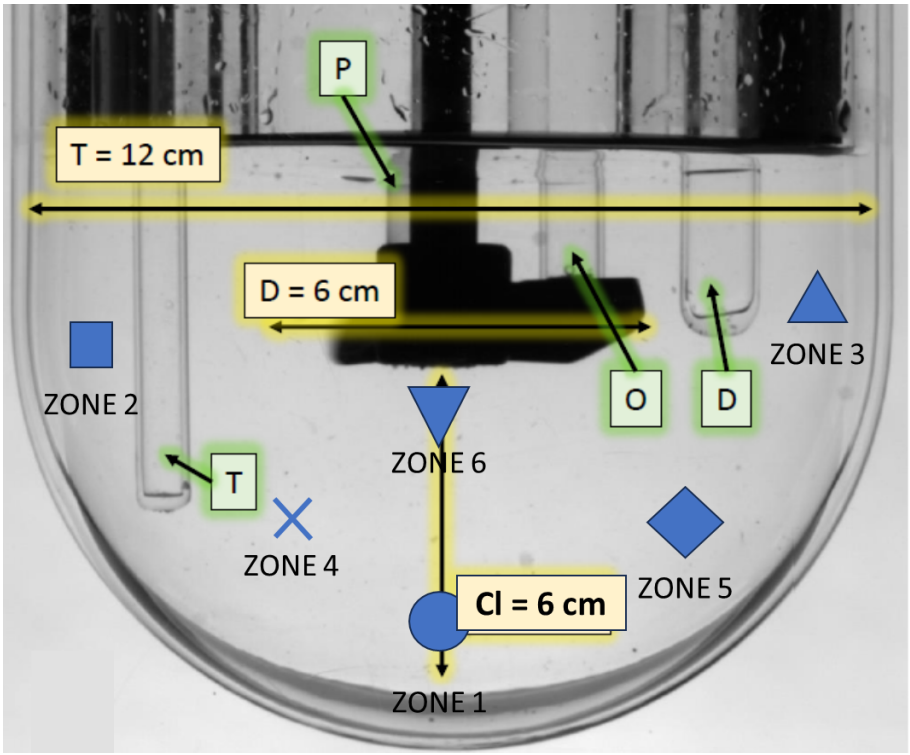


**Figure 1:** Description of the bioreactor setup. P, O, T and D (green elements, plunging) replace pH, dissolved oxygen, temperature and dielectric probes respectively.

the microcarrier suspension was homogeneous when agitated at $N = 1.7 \times N_{ref}$ and thus local concentrations were all equal to mean concentration $\langle C \rangle$. A $3^{rd}$ degree polynomial model was then fitted to calibrate the measured concentration $C$ based on the logarithm of the measured light intensity for each pixel, over the entire height of the liquid. As previously established by Delafosse et al. (2018), the linearity between attenuation $A$ and the concentration of particles was obtained only for volume fractions lower than 15 % (C = 7.5 g/L). For higher volume fractions, linearity is no longer obtained, probably because of light diffraction phenomena within the bed of particles, although this hypothesis has not been demonstrated. More details regarding the calibration step can be found in the paper of Delafosse et al. (2018). Post-processing of the data was performed using Matlab. Calibration results are detailed for 6 specific pixels, located in 6 specific zones of the vessel as shown in Figure 2. A mean absolute error of approximately 0.24 g/L was obtained from the $3^{rd}$ degree polynomial fit of the local microcarrier concentration for all concentrations and zones 1 through 6. This demonstrated the robustness of the technique, especially for intermediate and high particle concentrations. For lower concentrations experimental error can be explained by the fact that the measurements can be disturbed by variations in back-light intensity, room light intensity, or sensor sensitivity. Therefore, caution should be exercised

when analyzing data obtained for small particles concentrations (approximately $\langle C \rangle \leq 1$ g $L^{-1}$). Concerning the transient resuspension study, the first frame in which the agitator was found to be moving was manually determined in each condition and used to initialize the time variable.

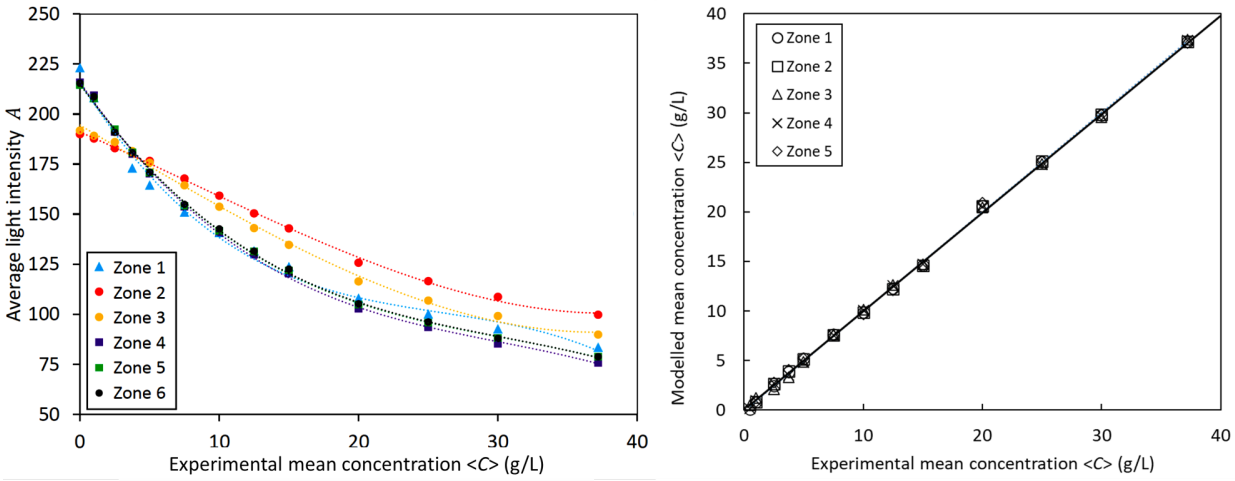


**Figure 2:** Calibration visualization for 6 defined zones of interest at 120 rpm for particle concentrations between 0 and 37.2 g $L^{-1}$.

## 3. Results and discussion

### *3.1. Local concentration distribution evolution over time $C(x, y, t)$*

Videos were taken during the suspension of microcarriers at different concentrations to evaluate suspension kinetics based on the average microcarrier concentration in the tank $\langle C \rangle$. Starting from a fully settled particle bed, agitation was then turned on at either 70 or 120 rpm and image acquisition was started. The agitation rate of $N_{ref} = 70rpm$ was chosen as particles were suspended for all particle concentrations and the agitation rate of 120 rpm was used to compare the dynamics of particle re-suspension at a higher rate. The spatial distribution of concentrations was determined frame by frame and for each pixel inside the bioreactor $C(x, y, t)$ from beginning of impeller rotation. It should be noted that the calibration was performed for concentrations between 0 and 37.2 g $L^{-1}$. Consequently, data points with measured concentrations outside this range were estimated by extrapolation of the polynomial relationships defined within the range. An example of the concentration distributions in the bioreactor described in Figure 1 obtained at 3 different times during the re-suspension is shown in Figure 3 (in this figure, the color bar indicates the local level of the particle concentration). As shown in the left part of this figure, microcarriers are initially settled at the bottom of the tank. After 40 seconds of suspension, the microcarriers

accumulated at the bottom were dispersed in the tank, reducing the bed depth. After approximately 80 seconds of suspension, a higher fraction of the particles have dispersed throughout the tank volume, further reducing the fraction of settled particles.

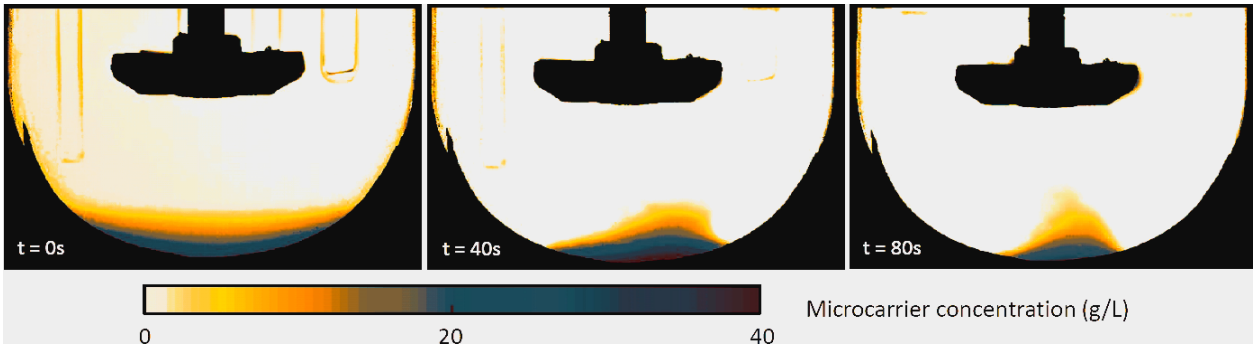


**Figure 3:** Concentration distribution obtained at 70 rpm after 0, 40 and 80 seconds of agitation. Microcarrier average concentration $\langle C \rangle$ was 2.5 g $L^{-1}$.

### *3.2. Local concentration evolution over time in 6 defined zones of interest*

Qualitatively, observing how microcarrier concentration evolves over time in certain defined STR zones (such as the 6 Zones defined in Figure 2) can be a good indicator of particle suspension characteristics. The time evolutions of particle concentrations in 6 zones of interest defined in Figure 2 are presented in Figure 4. Mean concentrations $\langle C \rangle$ ranged from 2.5 to 15 g $L^{-1}$ and agitation was kept constant at 70 rpm. Similar profiles were obtained between Zones 2 and 3 and between Zones 4 and 5 which are symmetrically opposite zones in the tank for all tested concentrations. The observed profiles within each zone were found to depend on the average microcarrier concentration in the system, specifically concerning the time to achieve an apparent steady state. The impact of particle concentration was the most pronounced in Zone 1 near the bottom of the tank where significant variations in homogenization time were observed. It is interesting to note that the time it took for the first particles to reach the highest zones near the top of the STR (Zones 2 and 3) typically depended on microcarrier concentration, probably since conditions with high microcarrier concentrations have a higher bed, reducing the time for particles to reach the top of the bioreactor. This visual representation led to the identification of different suspension steps and dynamics depending on the local zone observed and on microcarrier average concentration $\langle C \rangle$.

- To begin with, several steps during re-suspension were observed for small particle concentrations in zones very close to the bottom of the tank (Zone 1, $\langle C \rangle \leq 10$ g $L^{-1}$).

Initially, microcarrier concentration in that zone remained constant and higher than the average microcarrier concentration in the system. Once the agitation is turned on, a densification phase is observed, possibly due to fluid movements generated downwards by the impeller. It can be noted that the over-concentrations at this stage can be significant (reaching approximately 10 times the average concentration in the system during approximately 1 - 2 minutes for $\langle C \rangle$ of 2.5 g $L^{-1}$). Lastly, in these zones, particles were eventually progressively dispersed in the tank and a gradual decrease in particle concentration is observed until a stationary regime is obtained (for which the local concentration reaches the average concentration in the system $\langle C \rangle$). As it can be seen with the results presented for Zone 1, the time it takes to fully homogenize the system increased with microcarrier concentration (while it seemed to take approximately 100 seconds to homogenize Zone 1 for microcarrier concentrations of 2.5 g $L^{-1}$, it took over 400 seconds for microcarrier concentrations of 10 g $L^{-1}$).

- A second suspension trend was observed in zones 4, 5 and 6 which are situated just below the impeller. For high enough particle concentrations, these zones are situated in the bed of particles at the beginning of the experiment (zones 4-6 with particle concentrations $7.5 \leq \langle C \rangle \leq 15$ g $L^{-1}$) illustrates this trend. An initial phase was observed with particle concentrations higher than the average concentration (due to the fact that these zones are inside the initial particle bed), followed by a second stage where the particle concentration gradually decreased during homogenization until reaching the average concentration in the system $\langle C \rangle$. It can be noted at this stage that this zone attained degrees of homogenization much quicker than the previously described Zone 1 for example at a concentration of 10 g $L^{-1}$ (concentration of Zone 6 was close to $\langle C \rangle$ after approximately 200 seconds while Zone 1 reached these concentrations after approximately 400 seconds).

- The last suspension trend concerns zones which are not initially in the microcarrier bed (zones 2 and 3 for all concentrations studied, zones 4, 5 and 6 for $\langle C \rangle < 7.5$ g $L^{-1}$). In these cases, particle concentration gradually increases from 0 (*i.e.* clear liquid) to the average concentration $\langle C \rangle$. The homogenization of this zone was found to take approximately the same time as the presented Zone 1 at the same microcarrier concentration of 2.5 g $L^{-1}$ (approximately 100 seconds). However, much lower concentration variations were reported during this time (concentration range stayed within 0

and 2.5 g $L^{-1}$ in Zone 6 while varied between 2.5 and 20 g $L^{-1}$ in Zone 1).

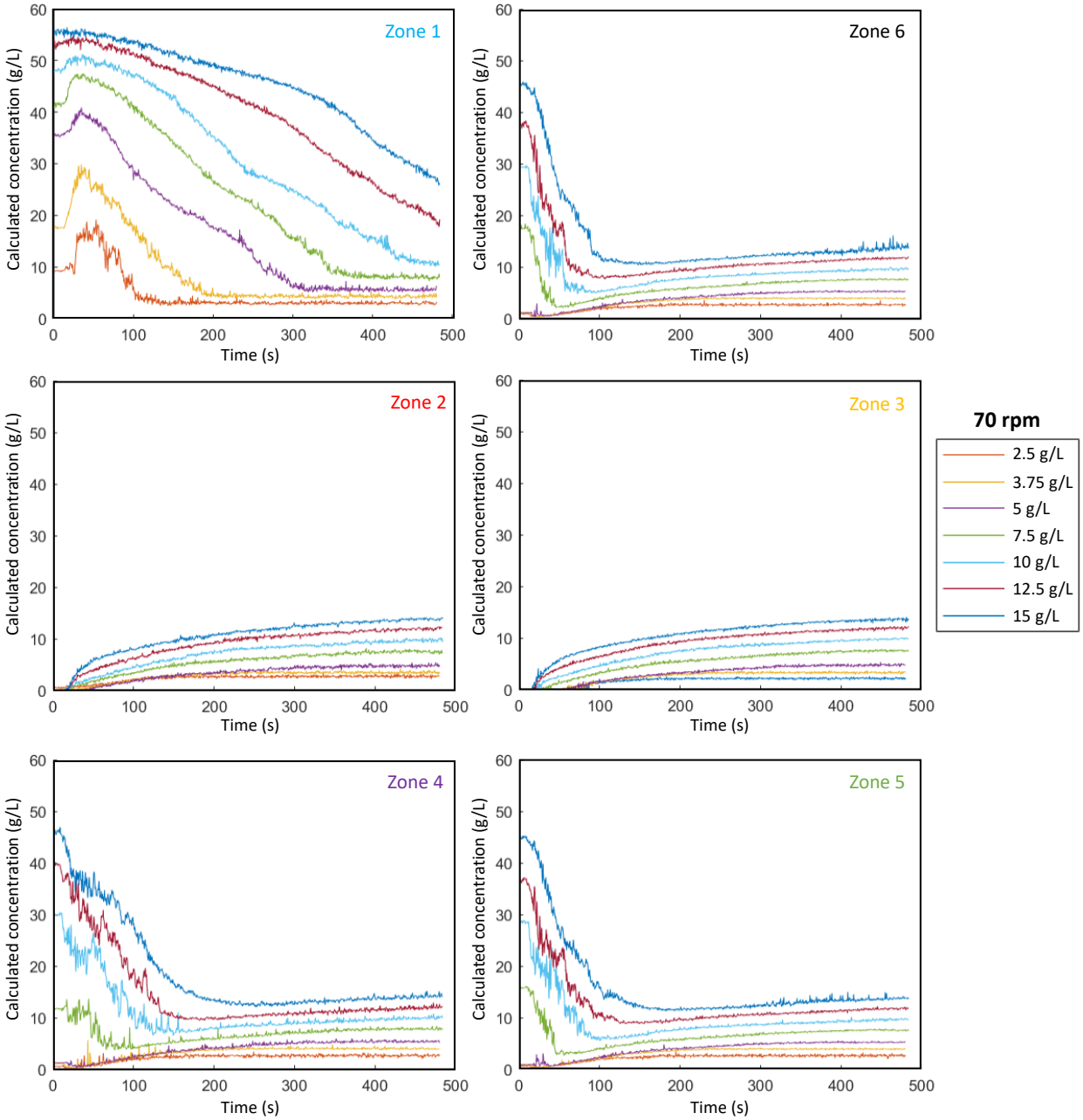


**Figure 4:** Temporal evolution of concentrations in Zones 1 to 6 (defined in Figure 2) during suspension at N = 70 rpm.

The results presented above indicated that the temporal evolution of particle concentration will have different profiles depending on the tank region. Specifically, the duration required to attain homogenization, as well as the maximal local concentration attained during suspension, seemed to depend on the local zone studied. Importantly, certain zones such as Zone 1 may be subject to significantly higher concentrations (up to a factor of 10) than the final average concentration for approximately 1 - 2 minutes due to an initial phase of compression generated by the impeller. Since the physical frictions and the shocks that

cells grown on microcarriers will be subject to ultimately depend on the time spent in specific high-concentration or low-concentration zones, it is important to further quantify these phenomena.

*3.3. Time evolution of the spatial distribution of the local heterogeneity index $\sigma(x, y, z, t)$*

The concentration evolution results were then extrapolated into a heterogeneity index $\sigma(x, y, t)$ which represents, for each pixel $(x, y)$ and for each time step $t$, the difference between the measured concentration $C(x, y, t)$ and the average final concentration $\langle C \rangle$. Results were normalized according to $\langle C \rangle$ in order to easily compare experiments performed at various concentrations (Equation 1). Theoretically, the evolution of this factor should ultimately tend towards 0 while the system tends towards a theoretically homogeneous state for which the concentration in every pixel tends towards the average concentration in the system $\langle C \rangle$.

$$\sigma(x, y, t) = \frac{|C(x, y, t) - \langle C \rangle|}{\langle C \rangle} \tag{1}$$

The spatial distribution of the heterogeneity index after 40, 80 and 160 seconds of resuspension with an average concentration $\langle C \rangle$ of 2.5 g $L^{-1}$ and with an agitation of 70 rpm are reported in Figure 5. On these figures, the local heterogeneity index was quantified using a color bar ranging from blue (for which $C(x, y, z) = \langle C \rangle$) to yellow (for which $C(x, y, z) \geq 5 \times \langle C \rangle$) These results can be compared to Figure 3 for which the same data are used and only the measured concentration represented. It can be observed that large portions of the bioreactor have a heterogeneity index of suspension between 0 and 1 after 40 and 80 seconds. This indicates that, in the majority of the STR, the concentration remains in a range of 0 and 2 times $\langle C \rangle$. However, notable zones were found to have concentrations which were measured as high as over 5 times $\langle C \rangle$. These zones typically correspond to zones in the hemispherical bottom of the STR. The heterogeneity index was found to be quite uniformly distributed and close to 0 after 160 seconds of suspension at 70 rpm and $\langle C \rangle = 2.5$ g/L.

Lastly, the same results obtained with an agitation of 120 rpm can be found in Figure 6. Contrary to the results obtained at $N_{ref}$, agitating at 120 rpm indicated, as expected, a much quicker homogenization of particles. In the presented experiment at a $\langle C \rangle$ of 2.5 g $L^{-1}$, almost the entire tank was found to be homogenized after only 40 seconds, whereas this degree of homogenization was only achieved after 160 seconds when agitating at 70 rpm. The zones which were found to take the longest time to achieve the target concentration

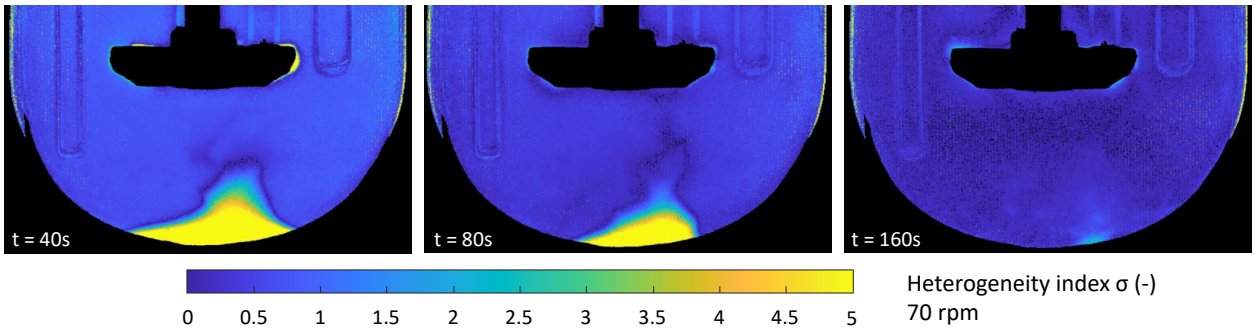


**Figure 5:** Heterogeneity index distribution evolution over time with a microcarrier concentration of 2.5 g $L^{-1}$ and agitation set to 70 rpm. The distribution is presented after 40, 80 and 160 seconds of agitation.

were near the bottom of the tank under the impeller. It can also be noted that, at 120 rpm, the tank seemed to achieve a constant degree of homogenization after approximately 80 seconds (the distribution of $\sigma(x, y, t)$ was not found to significantly change between 80 and 160 seconds, indicating a steady regime).

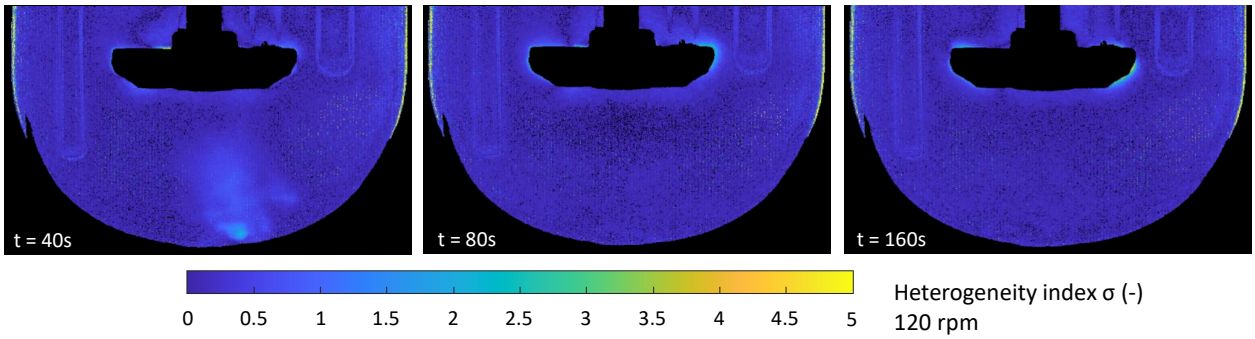


**Figure 6:** Heterogeneity index distribution evolution over time with a microcarrier concentration of 2.5 g $L^{-1}$ and agitation set to 120 rpm. The distribution is presented after 40, 80 and 160 seconds of agitation.

### *3.4. Average heterogeneity index evolution over time* $\langle\sigma(t)\rangle$

For each time step $t$, the average value of $\sigma(x, y)$ was calculated as an average over all of the pixels in the bioreactor $N_{pixel}$. Accordingly, the average heterogeneity index $\langle\sigma(t)\rangle$ was calculated using Equation 2.

$$\langle\sigma(t)\rangle = \sum_{N_{pixel}} \frac{\sigma(x, y, t)}{N_{pixel}} \tag{2}$$

The asymptotic value $\langle\sigma(t \to \infty)\rangle$ of $\langle\sigma(t)\rangle$ was removed from the values of $\langle\sigma(t)\rangle$ for the purposing of plotting. Results concerning this homogeneity index are presented in Figure 7 for both agitation rates of 70 (left) and 120 rpm (right). For the lowest mean concentration $\langle C\rangle = 2.5$ g/L, a wider scatter of the data is observed. This is probably due

to the value of the absolute experimental error (0.24 g/L) and the intrinsic definition of $\sigma$. To begin with, increasing the average microcarrier concentration while maintaining the same agitation rate led to similar homogenization profiles but with different transient behaviours. For example, the time required to achieve a stable level of homogenization was found to be approximately 200 seconds with $\langle C \rangle$ of 2.5 g $L^{-1}$ whereas this duration gradually increased with concentration to achieve around 700 seconds when the $\langle C \rangle$ concentration was of 15 g $L^{-1}$. Such relatively high times of microcarrier homogenization are in accordance with preceding results obtained in bioreactors (Ibrahim and Nienow, 2004; Grein et al., 2016). Interestingly however, when increasing the agitation rate to 120 rpm, the homogenization time in all concentrations remained stable around 50 seconds. It seems that, for the range of concentrations tested, increasing the agitation rate to 120 rpm generated the un-correlation of agitation from particle concentration, or at least that this variation is not detected. Lastly, in both agitation conditions (70 and 120 rpm), $\langle \sigma \rangle$ seemed to also vary depending on the concentration when the system achieved a steady state.

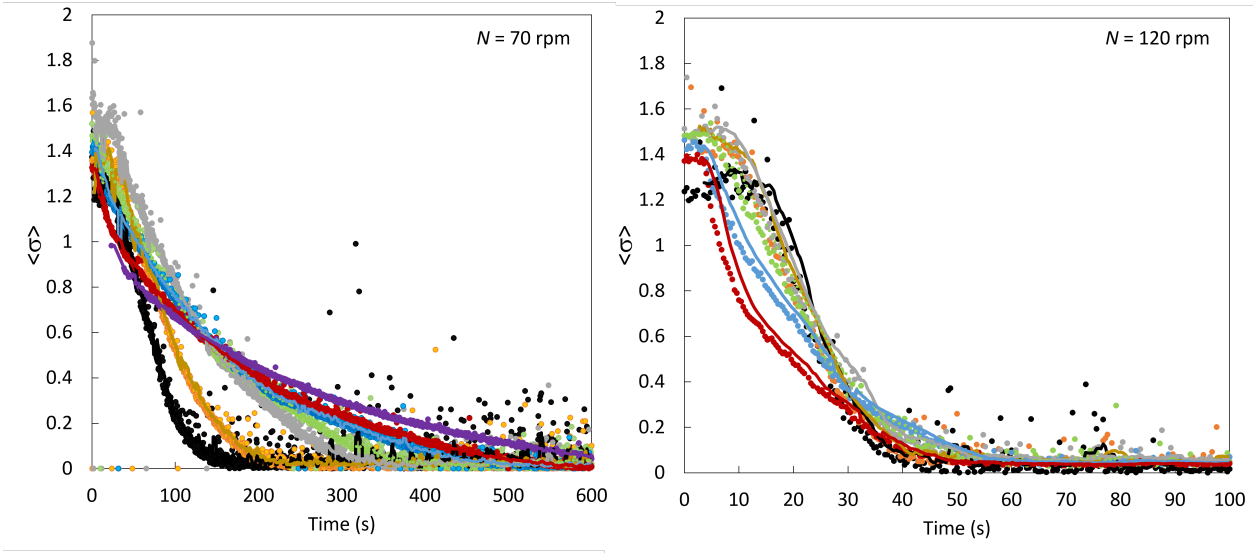


**Figure 7:** Evolution of the average heterogeneity index evolution over time $\langle \sigma(t) \rangle$. Concentrations ranged between 2.5 and 15 g $L^{-1}$. Agitation rates are 70 (left) and 120 (right) rpm. Concentrations of microcarriers are • 2.5 g/L, • 3.75 g/L, • 5 g/L, • 7.5 g/L, • 10 g/L, • 12.5 g/L, • 15 g/L. For a better readability, the experimental results were fitted using the mean value over 10 successive data.

### *3.5. Local homogenization duration $\tau(x, y)$*

The level of homogeneity in heterogeneous systems can be evaluated via various methods. A simple method consists in describing the time that it takes for a given system (or area) to achieve a certain level of homogeneity. For this, in each data point, the ratio between the

measured concentration $C$ and the average concentration $\langle C \rangle$ can be calculated. The time it takes the system to achieve a degree of homogenization, or local homogenisation time $\tau(x, y)$, can then be obtained from the data as an indicator to compare systems between each other, as reviewed in Ascanio (2015). To determine this homogenization duration, experimental data were smoothed using the mean value of ten successive measurements. Then, the local homogenization duration $\tau(x, y)$ was defined as the time necessary for $\sigma(x, y, t)$ to remain in the interval $[0.95 \times \langle \sigma(t \to \infty) \rangle; 1.05 \times \langle \sigma(t \to \infty) \rangle]$. Results of $\tau(x, y)$ for concentrations ranging from 2.5 to 12.5 g $L^{-1}$ with an agitation rate of 70 rpm are presented in Figure 8 using a color map ranging from blue (fastest homogenization of particles) to yellow (slowest homogenization).

First, it can be observed that there is a spatial gradient within the tank concerning the duration to achieve the target concentration $\langle C \rangle$, regardless of the concentration in the tank. Typically, zones near the bottom of the tank were found to take longer to achieve the average concentration (represented in yellow and green). A gradient in homogenization duration is observed for all microcarrier concentrations, with durations lasting from nearly 0 to over 1000 seconds depending on microcarrier average concentration in the tank. For low microcarrier concentrations (2.5 g $L^{-1}$), most of the STR volume had homogenization durations between 0 and 200 seconds and quickly reached the target concentrations. This indicates that for these particle concentrations, agitating at 70 rpm for approximately 300 seconds could ensure that the majority of the tank volume achieved the target concentration. However, when increasing microcarrier concentration over 5 g $L^{-1}$, most of the tank volume had values of $\tau$ above 300 seconds, and notable zones which were difficult to homogenize at the bottom of the tank. In these cases, a homogenization of 300 s at 70 rpm would be insufficient to successfully suspend the particles. Homogenization durations may take up to 900 s in these cases.

### *3.6. Statistic distribution of the homogenization duration $\tau(x, y)$ within the tank*

Globally, the knowledge of homogenization duration is important to quickly compare the performance of particles re-suspension and help to size agitation processes. However, despite the mean value of homogenization time is generally looked for, some significant spatial discrepancies may be observed in the tank. To complete the preceding information provided by graphical plots, the spatial distribution of $\tau$ was observed at 70 rpm according to the average concentration in the tank using box-plots (Figure 9). An increase in $\tau$ with increasing concentration which was observed spatially in the previous paragraph is also observed in the

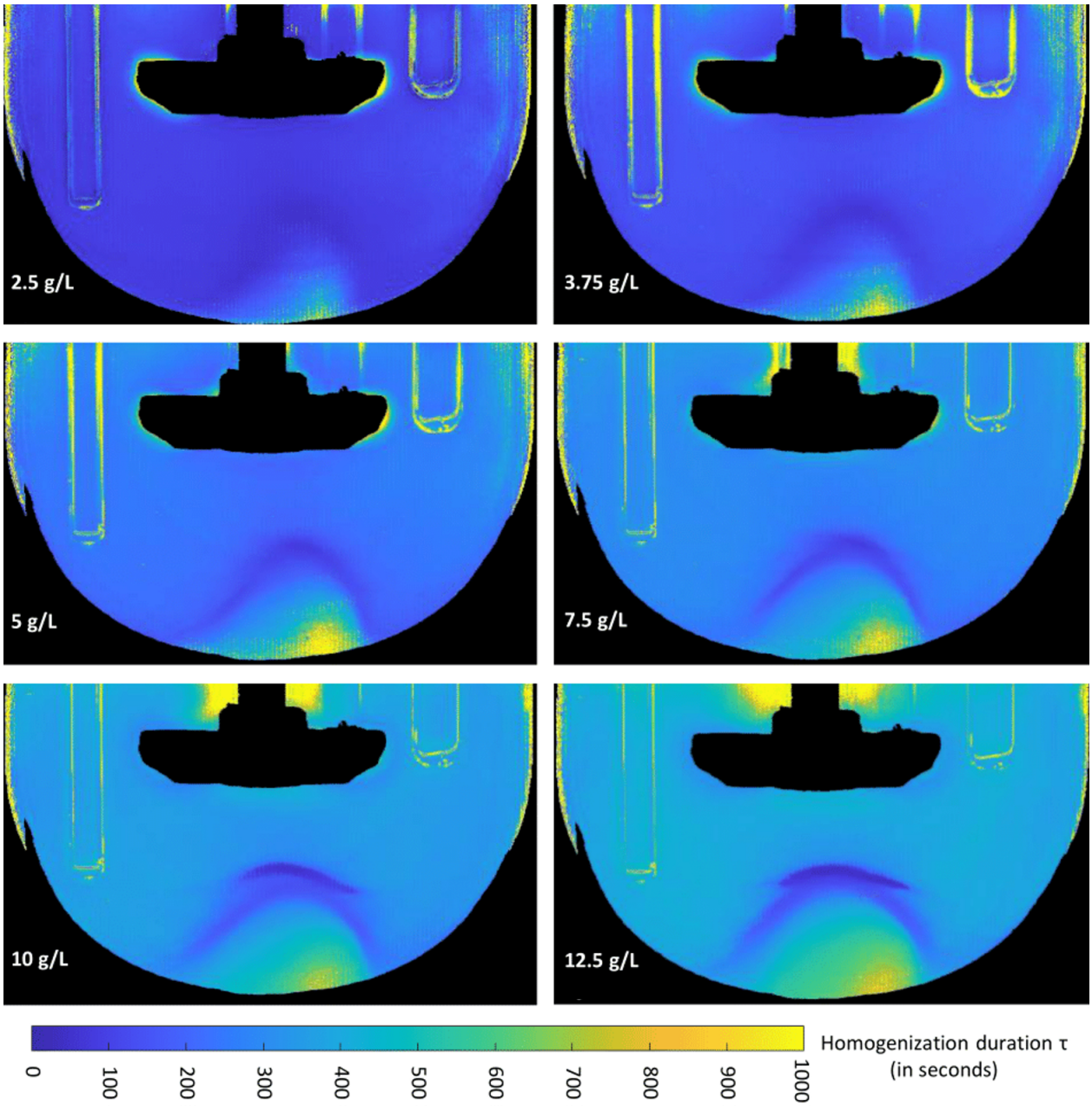


**Figure 8:** Local homogenization time $\tau(x, y)$ calculated for various average microcarrier concentrations during suspension at 70 rpm.

distribution plots of $\tau$. Whereas the median duration to achieve a 'homogeneous state' was of 112.8 seconds when $\langle C \rangle$ was 2.5 g $L^{-1}$, this value was multiplied by over a factor of three (446 seconds) with $\langle C \rangle$ of 15 g $L^{-1}$. In addition, the same experiments were performed at 120 rpm for which the homogenization time is represented according to the average concentration in the STR in Figure 9. When increasing the agitation in the tank, the average value of $\tau$ was not only found to be lower but also the distribution was found to be less disperse for all concentrations indicating that there may be less spatial heterogeneity during suspension when agitating particles at a higher agitation rate. Interestingly, these results also tend to demonstrate that the average homogenization duration in the STR becomes independent

from microcarrier concentration when increasing agitation. In order to minimize the duration of homogenization, it may be of use to increase the agitation rate above $N_{ref}$ to, as expected, limit homogenization time and interestingly the time during which spatial heterogeneities of particle concentrations are observed, particularly if particle concentrations are high.

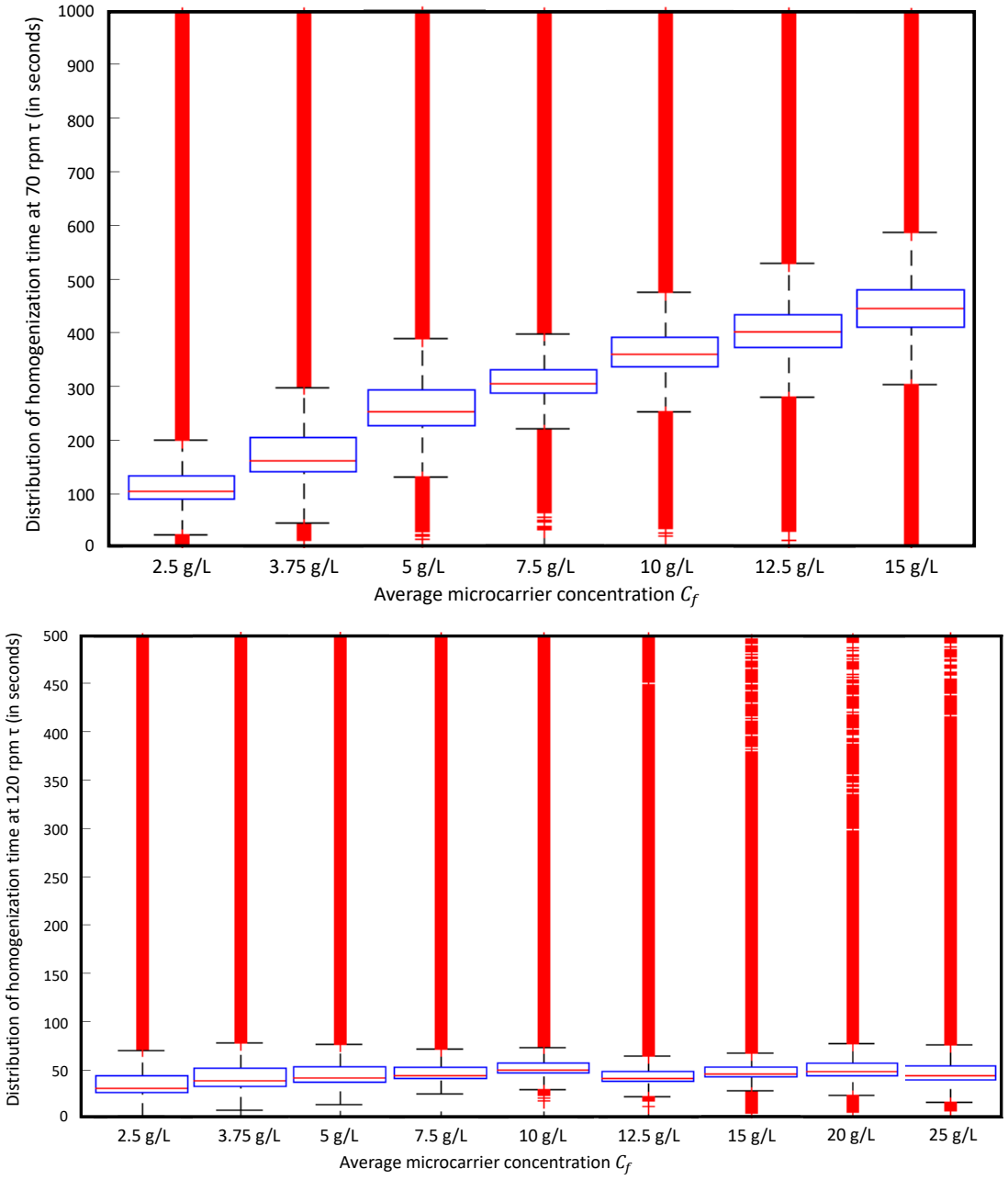


**Figure 9:** Statistic distribution of the homogenization time $\tau$ measured in the tank at different microcarrier concentrations for an agitation above $N_{ref}$. Agitation was set to 70 (top) and 120 (bottom) rpm.

### *3.7. Local over-concentration index during particle re-suspension $\gamma(x, y, t)$*

In order to have information not only on the duration but also on local concentration ranges in the bioreactor, a separate analysis of the data was performed. For each pixel, the

measured concentration in each frame $C(x, y, t)$ was compared to the average concentration $\langle C \rangle$. In cases where the measured concentration was above the average concentration, local over concentration index $\gamma(x, y, t)$ was set to the level of over-concentration normalized according to $\langle C \rangle$. If the measured local concentration was below the average concentration $\langle C \rangle$, the over-concentration factor was set to 0 (Equation 3). Accordingly, $\gamma(x, y, t)$ represents, for each time-point, a measure of the local over-concentration which could be correlated with increased particle collision probability when compared to an average value $\langle C \rangle$. In this sense, the temporal evolutions of the parameter $\gamma(x, y, t)$, even if they are qualitatively similar to the temporal evolutions of $\sigma(x, y, t)$, should be related to possible cell damage due to local microcarrier frictions or collisions and thus bring complementary data to the distribution of $\sigma$.

An example of the evolution of the spatial distribution of $\gamma(x, y, t)$ for $\langle C \rangle$ of 2.5 g $L^{-1}$ is presented in Figure 10 after 40, 80 and 160 seconds of agitation. As it could be expected, the zones which are overly concentrated during suspension concern zones near the bottom of the tank where particles were initially settled. In addition, as it has been described previously, certain zones near the reactor bottom experiment high particle concentration variations for which the local concentration can reach up to 10 times the average concentration in the system. These match previous observations where certain zones of the STR were found to be subject to certain levels of densification during suspension caused by the downwards fluid movement (Figures 3 to 5). Here, it should be also kept in mind that the calibration of the attenuation was calibrated for concentrations between 2.5 and 37.2 g/L ; higher concentrations are determined by extrapolating the model established for each pixel.

$$\gamma(x, y) = \begin{cases} \frac{C(x,y,t) - \langle C \rangle}{\langle C \rangle} & \text{if } C(x, y, t) > \langle C \rangle \\ 0 & \text{if } C(x, y, t) \leq \langle C \rangle \end{cases} \tag{3}$$

*3.8. Average over-concentration index during particle re-suspension $\langle \gamma(t) \rangle$*

From a global perspective, the integration of over-concentration factors $\gamma(x, y, t)$ can be calculated for all of the pixels in the reactor $N_{pixels}$. As a result, a global measure of the total over-concentration $\langle \gamma(t) \rangle$ present inside the STR can be estimated according to Equation 4 and the evolution of $\langle \gamma(t) \rangle$ can be observed over time to visualize the duration during which microcarriers will be subject to high levels of over-concentrations.

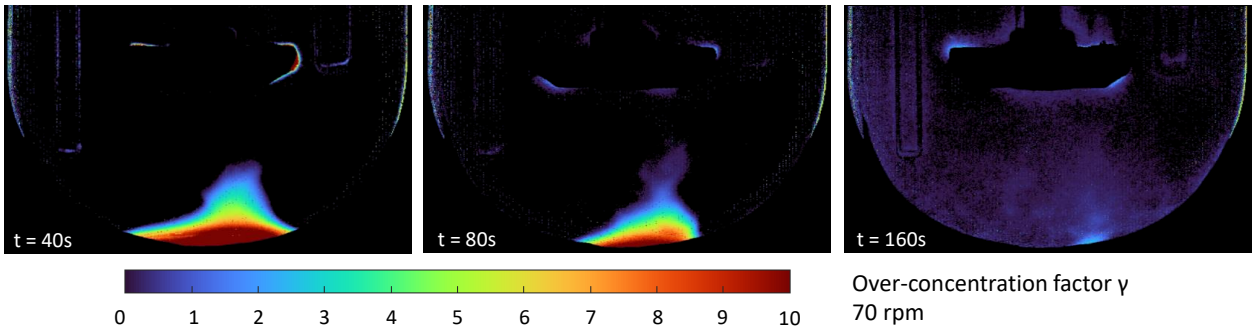


**Figure 10:** Over-concentration factor $\gamma(x, y, t)$ calculated for an average microcarrier concentration of 2.5 g $L^{-1}$ at agitation rates of 70 rpm after 40, 80 and 160 seconds of suspension.

$$\langle \gamma(t) \rangle = \sum_{N_{pixel}} \frac{\gamma(x, y, t)}{N_{pixel}} \tag{4}$$

The evolution of $\langle \gamma(t) \rangle$ is presented in Figure 11 for agitations of 70 rpm (left) and 120 rpm (right). As already indicated, for the lowest mean concentration $\langle C \rangle = 2.5$ g/L, a wider scatter of the data is observed which is possibly the consequence of the value of the absolute experimental error (0.24 g/L) and the intrinsic definition of $\gamma$. At agitation close to $N_{ref}$, the time during which the STR is subject to important levels of over-concentration seems to be increased, possibly since homogenization takes longer. Interestingly however, the time during which zones of the reactor are subject to over-concentrations, as well as the levels of over-concentration, were found to be similar for all concentrations tested when agitating at 120 rpm. Accordingly, increasing agitation during suspension may be an interesting way to minimize the time during which over-concentrations are present in the STR (which may potentially damage cells).

### *3.9. Time-accumulated over-concentration during particle re-suspension* $\Gamma$

The last step consisted in integrating the values of $\langle \gamma(t) \rangle$ in order to compare suspension profiles between each other. For this, the values of $\langle \gamma(t) \rangle$ were integrated until a steady state was obtained in the STR ; beyond this time, it was supposed that the contribution to $\Gamma$ was negligible. The duration to achieve a steady state can be found in Table 1 and the overall time-accumulated over-concentration $\Gamma$ (s) was calculated according to Equation 5.

$$\Gamma = \int_0^{t_{steady}} \langle \gamma(t) \rangle dt \tag{5}$$

Results of the calculated $\Gamma$ factor are presented in Table 1. To begin with, for an agitation rate of 70 rpm, $\Gamma$ was found to increase with increasing microcarrier concentration indicating

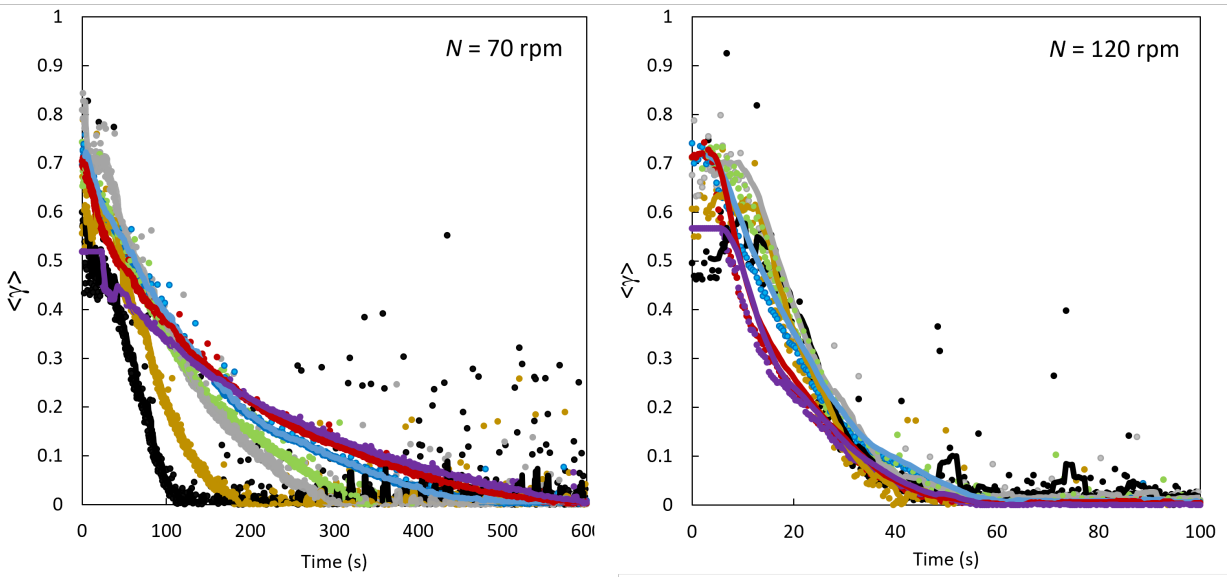


**Figure 11:** Average over-concentration index during particle re-suspension $\langle\gamma\rangle$ at 70 (left) and 120 (right) rpm. Concentrations of microcarriers are ● 2.5 g/L, ● 3.75 g/L, ● 5 g/L, ● 7.5 g/L, ● 10 g/L, ● 12.5 g/L, ● 15 g/L. For a better readability, the experimental results were fitted using the mean value over 10 successive data.

**Table 1:** Duration $t_{steady}$ to achieve a steady value of $\langle\gamma(t)\rangle$ according to agitation and microcarrier concentration and time-accumulated over-concentration factor $\Gamma$.

| **Average concentration** $\langle C\rangle$ (g $L^{-1}$) | $t_{steady}$ **at 70 rpm** (s) | $\Gamma$ **at 70 rpm** (s) | $t_{steady}$ **at 120 rpm** (s) | $\Gamma$ **at 120 rpm** (s) |
|---|---|---|---|---|
| 2.5 | 150 | 33.4 | 55 | 14 |
| 3.75 | 200 | 52 | 55 | 13.6 |
| 5 | 325 | 84 | 55 | 16.1 |
| 7.5 | 400 | 84 | 55 | 16.0 |
| 10 | 500 | 102.7 | 55 | 14.9 |
| 12.5 | 600 | 108.3 | 55 | 12 |
| 15 | 700 | 105.2 | 55 | 11.1 |

that the levels of over-concentration increased with $\langle C\rangle$. This was mainly the consequence of longer time required to attain suspension steady-state rather than differences in local $\gamma$ values. This trend is not visible for an agitation rate of 120 rpm, due to the fact that at this higher agitation rate, the homogenization time is much quicker and similar for all concentrations tested. Given a reasonable experimental error of 15 % in the determination of $\Gamma$, these results also suggested that $\Gamma$ was likely independent of microcarrier concentration at an agitation rate of 120 rpm. Interestingly however, the $\Gamma$ factors calculated were significantly lower for all of the concentrations tested with an agitation of 120 rpm. These results also indicated that the duration during which microcarriers are over-concentrated was much lower when increasing the agitation beyond $N_{ref}$.

However, an increase in agitation rate during the resuspension process may also imply an increase in microcarrier kinetic energy and collision frequency which may have significant

consequences on the viability of the adhered cells. It thus necessary to take into account these phenomena in the design of adapted agitation strategies for particles resuspension. To do this, it was here proposed to use the theory previously developed by Cherry and Papoutsakis (1988). For these authors, the severity of turbulent collisions TCS can be related to the particles local kinetic energy $E_c$, collision frequency $CF$, and volumetric solid fraction. Considering that particles have a similar size to the Kolmogorov's microscale of turbulence $\lambda_k$, their local velocity $v_p$ should be that of local turbulent eddies given by Equation 6.

$$v_p = (\nu\varepsilon)^{1/4} \quad \text{and} \quad E_C \propto v_p^2 \propto \varepsilon^{1/2} \tag{6}$$

with $\varepsilon$ the turbulent dissipation rate ($m^2/s^3$) (Kawase and Moo-Young, 1990). In the turbulent regime, it could also be considered that the agitator power number remained constant for the range of agitation rates and that the similitude $\varepsilon \propto N^3D^2$ is thus verified (Equation 7). This theory, essentially based on a volume averaged value of $\varepsilon$ was successfully used by Nienow et al. (2014) to improve the detachment of MSCs from microcarriers and by Nienow et al. (2016b) to determine the most suitable agitation conditions of MSC cultures. However, the spatial heterogeneity of the hydromechanical stresses in mixing tank has been intensively studied in the literature and well demonstrated. More precisely, the temporal evolution of the hydromechanical stresses encountered by the microcarriers was also modelled using an Euler-Lagrange Large-Eddy Simulation (LES), showing significant temporal and spatial discrepancies (Berry et al., 2016). From a general point of view, in a geometrically similar bioreactor, it was also established that in the turbulent regime, the dimensionless distributions of the turbulent dissipation rates $\varepsilon^* = \varepsilon/(N^3D^2)$ were also similar. This was previously confirmed in a MSC-culture lab-scale bioreactor using LES (Collignon et al., 2016). In the present study, it could be considered that not only the power number but also the spatial distribution of dimensionless turbulent dissipation rate $\varepsilon^*$ are conserved for the two agitation rates in the same design of bioreactor. This meant that, it is a reasonable hypothesis to consider that $\varepsilon(x, y, z) = K(x, y, z)\langle\varepsilon\rangle$ with $K$ a proportionality constant that weakly depends on agitation rate and impeller design (Nienow et al., 2016b). The transposition of such hypothesis to the comparison of different bioreactor designs would probably need further analysis. In addition, based on the work of Cherry and Papoutsakis (1988), particle collision frequency CF is expected to be proportional to particle velocity $v_p$ (Equation 8).

$$E_C \propto N^{3/2} \tag{7}$$

$$CF \propto v_p \alpha^2 \propto \varepsilon^{1/4} \alpha^2 \propto N^{3/4} \alpha^2 \tag{8}$$

with $\alpha$ the volume fraction of microcarriers.

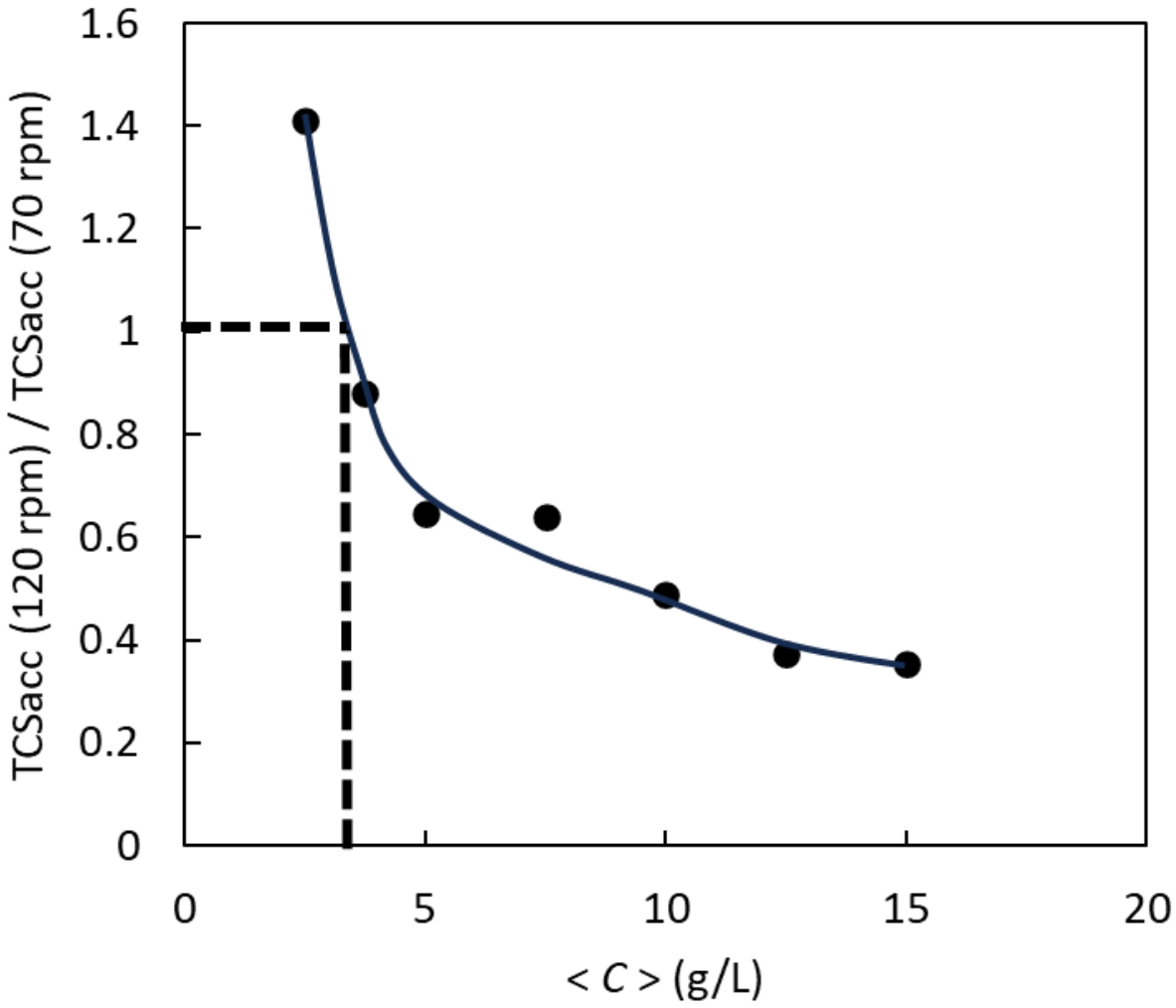


**Figure 12:** Evolution of TCSacc(120 rpm)/TCSacc(70 rpm) compared to microcarrier concentration

It was proposed here to take into account the integral effect of the heterogeneity of particle concentration during the transient suspension through $TCS_{acc}$ calculation. Accordingly, collisions severity, during the suspension time, can be estimated via Equation 9.

$$TCS_{acc}(N, \alpha) \propto E_C \cdot CF \cdot \Gamma \propto N^{9/4} \alpha^2 \Gamma \tag{9}$$

This type of approach integrates both collision intensities and an aspect of time during which cells will be exposed to such collisions. The comparison between the accumulated collision severity at 70 and 120 rpm during the suspension phase can be found in Figure 12 using the following equation:

$$\beta = \frac{TCS_{acc}(120, \alpha)}{TCS_{acc}(70, \alpha)} \propto \left(\frac{120}{70}\right)^{9/4} \frac{\Gamma_{120}}{\Gamma_{70}} \tag{10}$$

For the 2.5 g/L concentration, the relative error in the determination of the particle concentration was estimated to be about 10 % and it was previously shown that for this concentration, the scattering of the data was higher than for the other concentrations studied. The trend relating the ratio $\beta$ to the concentration of microcarriers should therefore be treated with caution for the lowest microcarrier concentration. The results indicated that the mean value of the microcarrier concentration had a significant effect on the ratio $\beta$ and that, depending on the value of the microcarrier concentration, it may be interesting to increase the resuspension agitation rate in order to reduce the time needed to resuspend all the particles and thus to limit $TCS_{acc}$. More precisely, our results suggested that, above 3 g $L^{-1}$, the ratio $\beta$ was less than 1, indicating that a higher agitation rate (here $N$=120 rpm) seemed to diminish the accumulated collision severity during suspension, compared to $N = 70$ rpm, confirming the possible interest of increasing the agitation during particle resuspension.

## Conclusion

The present study was dedicated to the implementation of the light attenuation technique to quantify the dynamics of solid particles suspended in a stirred tank. The effect of agitation frequency and particle concentration on homogenization time, heterogeneity index and particle overconcentration factor was studied. The results obtained showed that, for the configuration studied, the use of a stirring frequency slightly higher than the minimum particle suspension speed ($N_{ref} = 70$ rpm) generated homogenization times that could locally reach 1000 s, which is significantly higher than the mixing times of the liquid phase generally observed at this culture scale. Thus, during the phases of resuspension of the microcarriers, the possible need of suspension homogeneity should include this stirring time. It was also shown that, at $N_{ref} = 70$ rpm, the homogenization time was significantly influenced by the microcarrier concentration. Thus, in a fed-batch culture bioprocess with increasing microcarrier concentration, the time required for effective resuspension of the microcarriers would increase significantly (by about 100 s for $\langle C \rangle = 2.5$ g/L to more than 400 s for $\langle C \rangle$

= 15 g/L). From the point of view of the expected biological response, the adaptation of an interparticle collision model could show that a compromise must be found between the level of hydromechanical stresses generated (favored by a stronger agitation) and the duration of resuspension (accelerated by a more intense agitation). Here, a threshold concentration of 3 g/L was highlighted, above which it seems more favorable, from the point of view of interparticle collisions, to resuspend at a higher frequency. The generalization of this result to all types of bioreactor designs and scales will certainly require additional studies, since the steady-state spatial distribution of the particles for at the just-suspended state is significantly influenced by the design of the stirrer (Collignon et al., 2016).

Beyond these results, the choice between continuous or intermittent conditions arises when cultivating human cells, adherent or not, in a bioreactor. Samaras et al. (2019, 2020b,a) indeed showed that intermittent stirring conditions improved the efficiency of mixing the liquid phase. From a biological point of view, even if Tan et al. (2016) showed that MSC cultures were essentially carried out in continuous agitation (except during the initial adhesion phases and the steps of bead to bead transfer), Maillot (2022) showed during MSC cultures carried out in the same bioreactor as studied in the present study, that the application of an intermittent agitation throughout the culture significantly deteriorated the cell growth performance. This type of result is expected to vary depending on the biological specificities of the cultured cells. Samaras et al. (2018) indeed showed that during the cultivation of IPS cells, the differentiation of these cells into cardiomyocytes was favored by an intermittent agitation. Thus, the results of the present study confirm the potential impact of transient agitation strategies when implementing cell cultures in a bioreactor and the need to integrate these studies when looking for optimal productivity.

## References

Ascanio, G., 2015. Mixing time in stirred vessels: A review of experimental techniques. Chinese Journal of Chemical Engineering 23, 1065–1076.

Berry, J., Liovic, P., Šutalo, I., Stewart, R., Glattauer, V., Meagher, L., 2016. Characterisation of stresses on microcarriers in a stirred bioreactor. Applied Mathematical Modelling 40, 6787–6804.

Cherry, R.S., Papoutsakis, E.T., 1988. Physical mechanisms of cell damage in microcarrier cell culture bioreactors. Biotechnology and bioengineering 32, 1001–1014.

Collignon, M.L., Delafosse, A., Calvo, S., Martin, C., Marc, A., Toye, D., Olmos, E., 2016. Large-eddy simulations of microcarrier exposure to potentially damaging eddies inside mini-bioreactors. Biochemical engineering journal 108, 30–43.

Delafosse, A., Loubière, C., Calvo, S., Toye, D., Olmos, E., 2018. Solid-liquid suspension of microcarriers in stirred tank bioreactor – experimental and numerical analysis. Chemical Engineering Science 180, 52–63.

Discher, D.E., Janmey, P., Wang, Y.l., 2005. Tissue cells feel and respond to the stiffness of their substrate. Science 310, 1139–1143.

Ferrari, C., Balandras, F., Guedon, E., Olmos, E., Chevalot, I., Marc, A., 2012. Limiting cell aggregation during mesenchymal stem cell expansion on microcarriers. Biotechnology progress 28, 780–787.

Grangier, A., Wilhelm, C., Gazeau, F., Silva, A., 2020. High yield and scalable ev production from suspension cells triggered by turbulence in a bioreactor. Cytotherapy 22, S50.

Grein, T.A., Leber, J., Blumenstock, M., Petry, F., Weidner, T., Salzig, D., Czermak, P., 2016. Multiphase mixing characteristics in a microcarrier-based stirred tank bioreactor suitable for human mesenchymal stem cell expansion. Process Biochemistry 51, 1109–1119.

Harburger, D.S., Calderwood, D.A., 2009. Integrin signalling at a glance. Journal of cell science 122, 159–163.

Ibrahim, S., Nienow, A., 2004. Suspension of microcarriers for cell culture with axial flow impellers. Chemical Engineering Research and Design 82, 1082–1088.

Jossen, V., Schirmer, C., Mostafa Sindi, D., Eibl, R., Kraume, M., Pörtner, R., Eibl, D., et al., 2016. Theoretical and practical issues that are relevant when scaling up hmsc microcarrier production processes. Stem cells international 2016.

Kawase, Y., Moo-Young, M., 1990. Mathematical models for design of bioreactors: Applications of: Kolmogoroff's theory of isotropic turbulence. The Chemical Engineering Journal 43, B19–B41.

Maillot, C., 2022. Quantification and impact of microcarrier collisions during mesenchymal stem cell culture in bioreactors. Ph.D. thesis. University of Lorraine, France.

Maillot, C., De Isla, N., Loubiere, C., Toye, D., Olmos, E., 2022. Impact of microcarrier concentration on mesenchymal stem cell growth and death: Experiments and modeling. Biotechnology and Bioengineering 119, 3537–3548.

Maillot, C., Sion, C., De Isla, N., Toye, D., Olmos, E., 2021. Quality by design to define critical process parameters for mesenchymal stem cell expansion. Biotechnology Advances 50, 107765.

Nienow, A., Coopman, K., Heathman, T., Rafiq, Q., Hewitt, C., 2016a. Bioreactor engineering fundamentals for stem cell manufacturing, in: Stem cell manufacturing. Elsevier, pp. 43–75.

Nienow, A.W., Hewitt, C.J., Heathman, T.R., Glyn, V.A., Fonte, G.N., Hanga, M.P., Coopman, K., Rafiq, Q.A., 2016b. Agitation conditions for the culture and detachment of hmscs from microcarriers in multiple bioreactor platforms. Biochemical Engineering Journal 108, 24–29.

Nienow, A.W., Rafiq, Q.A., Coopman, K., Hewitt, C.J., 2014. A potentially scalable method for the harvesting of hmscs from microcarriers. Biochemical Engineering Journal 85, 79–88.

Papoutsakis, E.T., 1991. Fluid-mechanical damage of animal cells in bioreactors. Trends in Biotechnology 9, 427–437.

Piffoux, M., Nicolás-Boluda, A., Mulens-Arias, V., Richard, S., Rahmi, G., Gazeau, F., Wilhelm, C., Silva, A.K., 2019. Extracellular vesicles for personalized medicine: The input of physically triggered production, loading and theranostic properties. Advanced drug delivery reviews 138, 247–258.

Samaras, J.J., Abecasis, B., Serra, M., Ducci, A., Micheletti, M., 2018. Impact of hydrodynamics on ipsc-derived cardiomyocyte differentiation processes. Journal of Biotechnology 287, 18–27.

Samaras, J.J., Ducci, A., Micheletti, M., 2020a. Flow, suspension and mixing dynamics in dasgip bioreactors, part 2. AIChE Journal 66, e16999.

Samaras, J.J., Micheletti, M., Ducci, A., 2019. Suspension and mixing characterization of intermittent agitation modes in dasgip bioreactors. Chemical Engineering & Technology 42, 1587–1593.

Samaras, J.J., Micheletti, M., Ducci, A., 2020b. Flow, suspension, and mixing dynamics in dasgip bioreactors: Part 1. AIChE Journal 66, e17014.

Simaria, A.S., Hassan, S., Varadaraju, H., Rowley, J., Warren, K., Vanek, P., Farid, S.S., 2014. Allogeneic cell therapy bioprocess economics and optimization: Single-use cell expansion technologies. Biotechnology and bioengineering 111, 69–83.

Sion, C., Ghannoum, D., Ebel, B., Gallo, F., de Isla, N., Guedon, E., Chevalot, I., Olmos, E., 2021. A new perfusion mode of culture for wj-mscs expansion in a stirred and online monitored bioreactor. Biotechnology and Bioengineering 118, 4453–4464.

Sousa, M.F., Silva, M.M., Giroux, D., Hashimura, Y., Wesselschmidt, R., Lee, B., Roldão, A., Carrondo, M.J., Alves, P.M., Serra, M., 2015. Production of oncolytic adenovirus and human mesenchymal stem cells in a single-use, vertical-wheel bioreactor system: impact of bioreactor design on performance of microcarrier-based cell culture processes. Biotechnology progress 31, 1600–1612.

Stolberg, S., McCloskey, K.E., 2009. Can shear stress direct stem cell fate? Biotechnology progress 25, 10–19.

Tan, K.Y., Reuveny, S., Oh, S.K.W., 2016. Recent advances in serum-free microcarrier expansion of mesenchymal stromal cells: Parameters to be optimized. Biochemical and biophysical research communications 473, 769–773.

Wyrobnik, T.A., Ducci, A., Micheletti, M., 2020. Advances in human mesenchymal stromal cell-based therapies–towards an integrated biological and engineering approach. Stem Cell Research 47, 101888.

Wysotzki, P., Sancho, A., Gimsa, J., Groll, J., 2020. A comparative analysis of detachment forces and energies in initial and mature cell-material interaction. Colloids and Surfaces B: Biointerfaces 190, 110894.

Yourek, G., McCormick, S.M., Mao, J.J., Reilly, G.C., 2010. Shear stress induces osteogenic differentiation of human mesenchymal stem cells. Regenerative medicine 5, 713–724.

Yuan, Y., Kallos, M.S., Hunter, C., Sen, A., 2014. Improved expansion of human bone marrow-derived mesenchymal stem cells in microcarrier-based suspension culture. Journal of tissue engineering and regenerative medicine 8, 210–225.